Characterizing the Mechanism of the Double Proton Transfer in the Formamide Dimer

ARTICLE *in* THE JOURNAL OF PHYSICAL CHEMISTRY A · MARCH 2011

Impact Factor: 2.69 · DOI: 10.1021/jp111834v · Source: PubMed

5 AUTHORS, INCLUDING:

Esteban Vöhringer-Martinez
University of Concepción
21 PUBLICATIONS **269** CITATIONS
SEE PROFILE

Henry Lee Woodcock
University of South Florida
55 PUBLICATIONS **4,800** CITATIONS
SEE PROFILE

Alejandro Toro-Labbé
Pontifical Catholic University of Chile
223 PUBLICATIONS **4,365** CITATIONS
SEE PROFILE

THE JOURNAL OF PHYSICAL CHEMISTRY A

ARTICLE

pubs.acs.org/JPCA

Characterizing the Mechanism of the Double Proton Transfer in the Formamide Dimer

Jacqueline C. Hargis,*[,†,‡] Esteban Vöhringer-Martinez,[§] H. Lee Woodcock,[‡] Alejandro Toro-Labbé,[§] and Henry F. Schaefer, III[†]

[†]Center for Computational Quantum Chemistry, University of Georgia, Athens, Georgia 30602, United States

[‡]Department of Chemistry, University of South Florida, Tampa, Florida 33620, United States

[§]Laboratorio de Química Teórica Computacional (QTC), Pontificia Universidad Católica de Chile, Santiago, Chile

Supporting Information

ABSTRACT: The double proton transfer in the formamide dimer is characterized computationally by combining density functional theory and ab initio methods. The intrinsic reaction coordinate (IRC) is obtained at the B3LYP level of theory. Energies of several points along the IRC are treated by the more rigorous focal point method to test the validity of the B3LYP functional. The reaction mechanism is examined in terms of the energy profile, the reaction force, the chemical potential, and the reaction electronic flux. The energy profile for the activation process of the formamide dimer to the imino ether product obtained with the B3LYP functional is in agreement with the results of the focal point method. Together with the reaction force analysis and the reaction electronic flux a precise assignment of the structural and electronic contributions to the activation barrier becomes possible. The results show that the reaction starts with a structural rearrangement, where the two dimers approach each other, and is followed by electronic changes before the system reaches the transition state. This electronic contribution to the activation barrier steers the activation process. After the transition state is reached, deviations of the B3LYP functional from the more accurate focal point energies become apparent, where the errors may be rationalized in terms of the treatment of exchange. The inconsistency could be assigned to the incapacity of the functional to describe delocalization effects over the whole system.

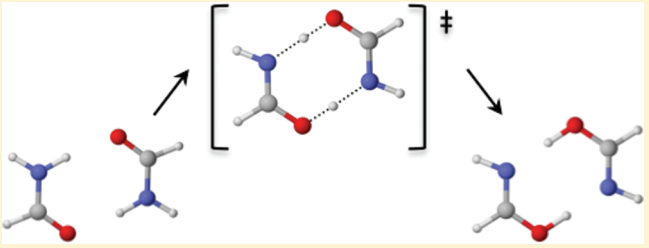

INTRODUCTION

Proton transfer is one of the most fundamental processes in chemistry and biology.[1−3] Multiple proton transfers, which occur either synchronously or asynchronously, have been found in proton relay systems in enzymes, hydrogen bonded water complexes, and prototropic tautomerisms. Double proton transfer in DNA base pairs is also a commonly cited example. The prototropic tautomerism of the formamide dimer is important in proteins and has been used as a model for nucleic bases.[4,5]

The formamide dimer has been studied extensively by theoretical[6−28] and experimental[29−31] methods. Despite the extensive work done on this system, the double proton reaction path has not to date been fully investigated. The study of Grabowski, Sokalski, and Leszczynski[28] examined the dimer at the MP2/6-311++G(d,p) level and concluded that the interaction of the formamide dimer has its largest component in the electrostatic term, while the less stable imino ether product is stabilized by the attractive delocalization term, where the electron correlation becomes more important. The methods in this study will be used to expand on this work exploring additional aspects of this system along the reaction path.

Several studies have examined the intrinsic reaction coordinate (IRC) to determine information about double proton transfer reactions. Cybulski and Sadlej[32] examined this process in the formamide−formic acid and the formamide−formamidine complexes. In that work they utilized the IRC method to monitor the changes in NMR parameters. Research by Toro-Labbé and coauthors[33−35] has utilized IRCs to explain reaction mechanisms examining energetic profiles together with reaction forces, chemical potentials, and reaction electronic flux.

In the present study the above methods will be combined with the focal point analysis scheme, to accurately describe the energy along the reaction path. Combining this with mechanistic investigations, a lucid picture may be painted to show the precise assignment of structural and electronic parts of the activation barrier. In addition, the performance of the B3LYP functional along the reaction coordinate will be analyzed.

THEORETICAL BACKGROUND

A chemical reaction takes place in multidimensional space and the characterization occurs by monitoring changes in geometrical parameters. The intrinsic reaction coordinate[36] (ξ) shows a

Received: December 13, 2010
Revised: February 4, 2011
Published: March 09, 2011

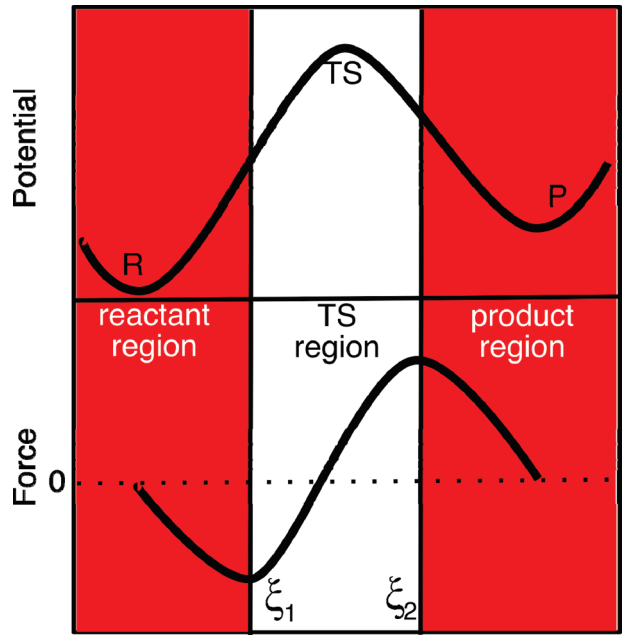

Figure 1. Schematic representation of the potential energy along the reaction coordinate for an elementary process and the reaction force providing the limits of characteristic regions of the reaction by its minimum and maximum.

projection of the multidimensional motion occurring in the chemical reaction. The energy profile along ξ corresponds to the minimum energy path relating reactants and products. Numerical differentiation of $E(\xi)$ results in the reaction force.[37,38]

$$F(\xi) = -\frac{dE}{d\xi}$$

Figure 1 shows a schematic representation of the potential energy along the reaction coordinate ξ for an elementary process and the corresponding reaction force. The reaction force is zero at reactants, transition state, and products and displays a minimum (ξ_1) and a maximum (ξ_2). These two extremes divide the reaction in three different regions: reactant region ($\xi_R \leq \xi < \xi_1$), transition state region ($\xi_1 \leq \xi \leq \xi_2$), and product region ($\xi_2 < \xi \leq \xi_P$).[33−35,37−47] In the reactant region the reactant undergoes mostly structural changes to achieve the reactive conformation at the force minimum. Once this conformation is reached, the electronic changes take over in the transition state region, resulting in bond formation and rupture. The region extends until the force maximum where a structural relaxation takes over to reach the product. These three region provide a framework, which allows a detailed analysis of the reaction mechanism, as has been shown for various reactions including intra- and intermolecular proton transfer,[33,34] S_N2,[44] and isomerization reactions.[43]

The chemical potential results from the Euler−Lagrange equation of the energy functional in density functional theory (DFT) as a Lagrange multiplier to conform with the stipulation that the electronic density integrates to N, the total number of electrons in the system.[48] For a N-electron system with total energy E and external potential $v(\vec{r})$, the chemical potential is defined as[48]

$$\mu = \left(\frac{\partial E}{\partial N}\right)_{v(\vec{r})} = -\chi$$

where χ is the electronegativity.[48−53] With the finite difference approximation the following working expression for the chemical potential is obtained,[48,51,52,54]

$$\mu \approx -\frac{1}{2}(I + A)$$

where I is the first ionization potential and A the electron affinity.

Calculation of the chemical potential for each structure along the reaction coordinate ξ yields $\mu(\xi)$. In previous works we have shown that variations of the chemical potential $\mu(\xi)$ are associated with electronic reordering in the system, which can be corroborated with changes in bond indices and natural charges.[33,34,43,44] These variations are quantified with the reaction electronic flux, which is defined as[33−35,43,44]

$$J(\xi) = -\frac{d\mu}{d\xi}$$

In analogy to thermodynamics, the reaction electronic flux can be used to describe the spontaneity of a process: positive values characterize a spontaneous change in the electronic density whereas negative ones a nonspontaneous one. The reaction electronic flux has evolved to be a very useful descriptor to identify the regions along the reaction coordinate that are characterized by electronic reordering and transfer. Therefore, it is complementary to the reaction force and enables a direct access and a better rationalization of the electronic changes along the reaction coordinate.

The focal point analysis is a two-dimensional extrapolation grid used to monitor the basis set and method dependence of the correlation energy to track the reaction energy toward the complete basis set full configuration interaction limit. This method, created by Allen and co-workers[55−58] was developed to examine chemical reactions at sub kcal mol^{-1} accuracy. However, in this case DFT geometries are used in conjunction with the focal point method[59] to attain accurate and affordable results appropriate for the current work.

COMPUTATIONAL DETAILS

Energies, structures, and transition states were initially determined using density functional theory employing the B3LYP generalized gradient approximation (GGA) exchange correlation functional. B3LYP combines Becke's description of exchange, the three-parameter HF/DFT hybrid exchange functional (B3),[60] and the dynamical correlation functional of definition Lee, Yang, and Parr (LYP).[61] The proton transfer reaction was followed with B3LYP and the 6-311G(d,p) basis set along the intrinsic reaction coordinate ξ, using mass-weighted internal coordinates and a step size of 0.01 a_0 $amu^{1/2}$. Reactants, transition state, and products were also optimized at the MP2/cc-pVQZ level for comparison. Stationary points were verified by harmonic vibrational analysis at the MP2 and B3LYP levels of theory.

The electronic chemical potential was obtained from single point energy calculations of the cationic and anionic forms of all structures along the reaction coordinate employing the B3LYP/6-311G(d,p) method. The Wiberg bond indeces were obtained from natural bond order analyses (NBO)[62,63] along the reaction coordinate using the NBO program[64] as implemented in the Gaussian 03[65] package.

A focal point analysis using the HF, MP2, CCSD, and CCSD(T) levels of theory was executed using the correlation consistent basis sets of Dunning[66] (cc-pVXZ, X = D, T, Q, 5) to

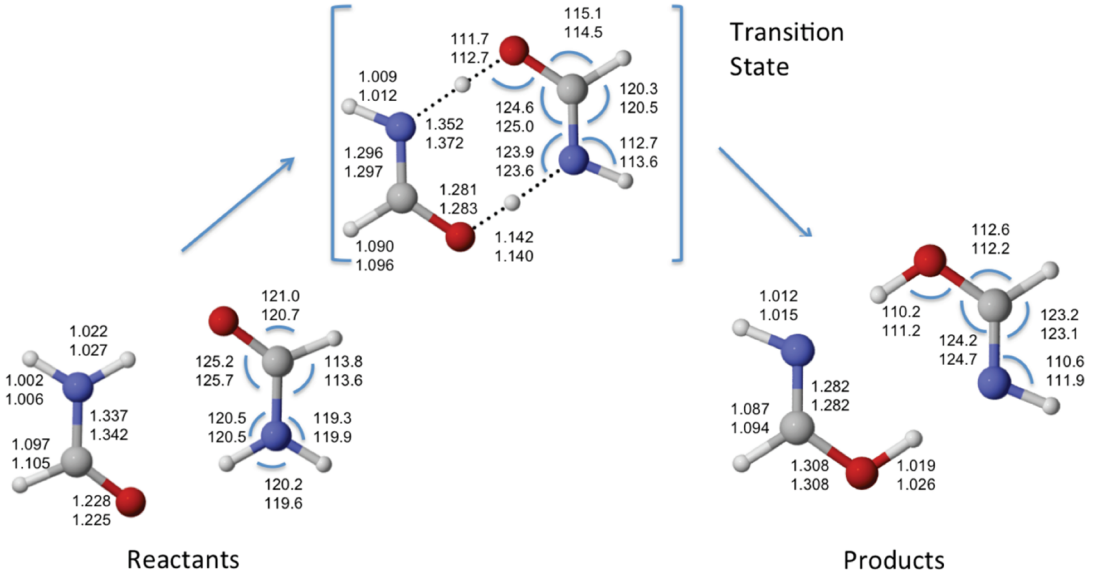

Figure 2. Schematic depiction of the formamide dimer undergoing the double proton transfer reaction. The bond distances in Ångstroms and the angles in degrees are shown for the MP2/cc-pVQZ (number on top) and the B3LYP/6-311G(d,p) (number at bottom) optimized geometries for reactants, transition state, and products.

yield values extrapolated to the basis set limit. This extrapolation method has proven effective in combination with DFT geometries;[59] therefore, the aforementioned B3LYP and MP2 geometries were utilized. The total energy extrapolation was partitioned in two terms (SCF and correlation energies). The first term, total SCF energy, was fitted to the functional form[67]

$$E_{\mathrm{SCF}}(X) = A + B\mathrm{e}^{-CX}$$

where X is the cardinal number corresponding to the maximum angular momentum of the basis set. A, B, and C are determined by these equations for the extrapolation of the Hartree−Fock energy.

$$A = E_3 - B\mathrm{e}^{-CX_3}$$

$$B = \frac{E_3 - E_2}{\mathrm{e}^{-CX_2}(\mathrm{e}^{-C} - 1)}$$

$$C = -\ln\frac{E_3 - E_2}{E_2 - E_1}$$

The correlation energy uses a different formula:[68]

$$E_{\mathrm{CORR}}(X) - E_{\mathrm{SCF}}(X) = A + BX^{-3}$$

where A and B are determined by these equations:

$$A = E_2 - BX_2{}^{-3}$$

$$B = \frac{E_2 - E_1}{X_2{}^{-3} - X_1{}^{-3}}$$

In the equations above, E_x corresponds to the energy of the largest basis sets computed at that level of theory. E_3 would be the largest basis set and E_2 and E_1 would correspond to the next to largest basis sets in descending order with X still being defined as the principal number in the Dunning correlation-consistent basis set. Hartree−Fock uses a three-point extrapolation and for levels of theory with electron correlation, including MP2, CCSD, and CCSD(T), a two-point extrapolation is used. The extrapolated values are additive, determining the final energy near the CBS limit. Molpro version 2006.1[69−71] was used for all energies computed in the focal point analyses. For the MP2 geometry optimizations Q-Chem 3.2[72] was used.

RESULTS AND DISCUSSION

The double proton transfer of the formamide dimer has been investigated here using several approaches. The most accurate determination of the barrier combined MP2/cc-pVQZ geometries (Figure 2) and the focal point extrapolation method. The 19.9 kcal mol^{-1} barrier (Table 1) between the reactant and the transition state ($\Delta E_{\mathrm{f}}^{\ddagger}$) shows that considerable energy is necessary for the double proton transfer to occur. Additionally, the product lies 16.8 kcal mol^{-1} higher in energy ($\Delta E_{\mathrm{reaction}}$) than the reactant. B3LYP/6-311G(d,p) geometries (Figure 2) and the focal point extrapolation method yield nearly the same results (Table 2). Using the 6-311++G(d,p) basis at the MP2 level, the work of Grabowski, Sokalski, and Leszczynski[28] determined the energy difference between the reactant, the transition state, and product to be 20.5 and 19.6 kcal mol^{-1}, respectively. DFT in the current work has difficulties yielding the correct energy in the product region, in contrast to the focal point method, which is able to describe the region accurately. There is a smaller discrepancy in the transition state region between the MP2 energies and the focal point energies.

B3LYP and focal point results (Table 2) yield a similar forward barrier ($\Delta E_{\mathrm{f}}^{\ddagger}$); however, there is discrepancy in the reverse barrier ($\Delta E_{\mathrm{r}}^{\ddagger}$). It has been shown that B3LYP underestimates reaction barriers,[73,74] so the perplexing behavior of B3LYP in this case is of interest. This behavior could allude to an error in the basis set, 6-311G(d,p). In the past, certain Pople basis sets have been shown to produce errors associated with intramolecular basis set superposition error;[75,76] however, 6-311G(d,p) was not highlighted as problematic. Current results agree; after computing B3LYP energies with several basis sets including the sizable cc-pVQZ basis set, we observe no significant differences

Table 1. Focal Point Table[a]

basis set	ΔE_e [RHF]	$+\delta$ [MP2]	$+\delta$ [CCSD]	$+\delta$ [CCSD(T)]	ΔE_e [CCSD(T)]
		(a) For the MP2/cc-pVQZ Barrier for Formamide Double Proton Transfer			
cc-pVDZ	29.44	−11.45	1.97	−1.64	18.32
cc-pVTZ	30.69	−12.45	2.49	−2.01	18.71
cc-pVQZ	31.12	−12.35	2.66	−2.03	19.40
cc-pV5Z	31.19	−12.22	[2.66]	[−2.03]	[19.60]
CBS limit	[31.21]	[−12.08]	[2.78]	[−2.04]	[19.87]
		$\Delta E^{\ddagger} = \Delta E_e$[CBS CCSD(T)] = **19.87 kcal mol^{-1}**			
		(b) For the MP2/cc-pVQZ Reaction Energy			
cc-pVDZ	21.68	−5.75	−0.28	−0.77	14.88
cc-pVTZ	22.72	−6.27	0.03	−0.96	15.52
cc-pVQZ	23.06	−6.02	0.15	−0.94	16.26
cc-pV5Z	23.12	−5.84	[0.15]	[−0.94]	[16.49]
CBS limit	[23.14]	[−5.65]	[0.24]	[−0.92]	[16.81]
		$\Delta E_{reaction} = \Delta E_e$[CBS CCSD(T)] = **16.81 kcal mol^{-1}**			
		$\Delta E_{reverse} = \Delta E^{\ddagger} - \Delta E_{reaction}$ = 19.87 kcal mol^{-1} − 16.81 kcal mol^{-1} = **3.06 kcal mol^{-1}**			
fit	$a + be^{-cX}$	$a + bX^{-3}$	$a + bX^{-3}$	$a + bX^{-3}$	additive
points (X)	3, 4, 5	4, 5	3, 4	3, 4	

[a] The remaining focal point tables will be supplied in the Supporting Information.

Table 2. Energy Barriers for the Forward Reaction, Reaction Energy, and the Reverse Barrier[a]

	MP2//focal point	B3LYP//focal point	B3LYP// B3LYP	B3LYP// HF
$\Delta E_f^{\ddagger}$	19.9	19.9	19.9	31.0
$\Delta E_{reaction}$	16.8	16.9	18.7	23.2
$\Delta E_r^{\ddagger}$	3.1	3.0	1.2	7.8

[a] The HF energies were computed using the B3LYP geometry.

(Supporting Information). Thus a problem with the B3LYP functional is more likely and has been investigated herein.

After the basis set is eliminated as a possible source of error, the remaining possibilities are the exchange or correlation used in the B3LYP functional. The diagnosis of this problem can be obtained by comparing the focal point and B3LYP results to Hartree−Fock barriers. To begin the analysis, the correlation is inspected. As expected, the barrier lowers when going from HF to the focal point results, which is attributed purely to correlation. Furthermore, most of the correlation is recovered when going from HF to MP2, as seen in Table 1. To monitor the effects of LYP correlation, NBO analyses were employed (i.e., HF vs HF-LYP). Orbital stabilizations as a function of reaction coordinate (i.e., hydrogen bonding, etc.) remained consistent with and without LYP correlation. This confirms that LYP correlation has a negligible impact on delocalization and nonbond interactions (vide infra).

It has been shown that B3LYP produces an overestimation of nonbonded repulsion in reactions involving rings and cagelike molecules.[77] Additionally, a B3LYP error exists that overestimates delocalization stabilization.[74,77,78] Due to the elimination of a basis set or correlation effect, altering the results of the B3LYP/6-311G(d,p) reaction profile, the problem must lie in the B3 exchange. The B3 exchange consists of 20% HF, 8% Slater exchange, and 72% B88. Again, using the HF results as a reference, one can monitor the effect of B88 by varying the amount incorporated.[78] The B88 exchange causes a significant drop in the transition state barrier with a drop in the product to a slightly lesser degree (Supporting Information). This is again confirmed using NBO analysis (i.e., HF vs B3-noLYP[79]) and examining the orbital stabilizations associated with the reaction coordinate; small differences are observed in reactant interactions (∼2 kcal mol^{-1}), large changes at the transition state (∼45 kcal mol^{-1}), and slightly smaller changes at the product (∼10 kcal mol^{-1}). This effect is exaggerated as the percentage of B88 exchange is increased and attributed to the overestimation of nonbonded repulsion. Hence, exchange in combination with delocalization leads to an underestimation of the forward barrier, whereas the nonbond repulsion leads to an increase in the forward barrier and the product energy. These counteracting factors explain the seemingly correct description of the forward barrier by B3LYP, while also explaining the erroneous reaction energy when the focal point is compared to DFT results.

To study the reaction mechanism of the double proton transfer in formamide, the intrinsic reaction coordinate between reactant and product was followed. Figure 3a shows the potential energy along the reaction coordinate at the B3LYP/6-311G(d,p) level. From the potential energy it can be determined that the double proton transfer occurs in a synchronous manner. The energy computed using B3LYP/6-311G(d,p) was benchmarked using nine points determined from focal point extrapolations assuming B3LYP geometries (see blue points in Figure 3a). There is significant agreement between the focal point benchmark and the energies computed with the B3LYP method. The primary disagreement appears to lie in the product region. The results of Grabowski, Sokalski, and Leszczynski[28] show the main contribution to the interaction energy in the product (the imino ether form) is attributed to the delocalization energy over the entire dimer.

The reaction force profile leads to intriguing information about the double proton transfer of the formamide dimer. As shown in Figure 3b, the reaction force profile is linear from the reactant until close to the minimum of the force, where a pronounced decrease sets in. This linear decrease is due to the monomers decreasing their intermolecular distance to each other with no changes in the distance of the N−H bond, as shown in Figure 3c. The negative linear decrease of the reaction force

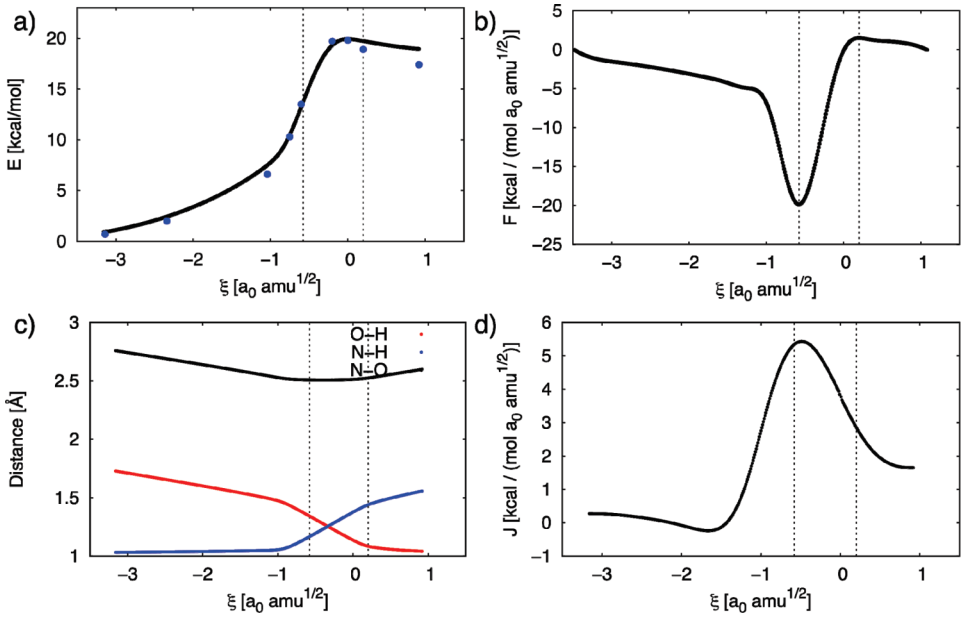

Figure 3. (a) Potential energy along the intrinsic reaction coordinate computed with the B3LYP/6-311G(d,p) method in comparison to focal point energy analysis of characteristic geometries (blue circles). (b) Reaction force and the dashed lines showing the minimum and maximum of the reaction force. (c) Distance between the nitrogen or oxygen atom and the transferred hydrogen atom, and the nitrogen−oxygen distance representing the approximation of the two monomers. (d) Reaction electronic flux obtained as the derivative of the chemical potential along the reaction path.

implies a repulsion energy, which depends quadratically on the distance between the two monomers, suggesting an interaction similar to the one in a covalent chemical bond. The pronounced decrease near the minimum initiates the elongation of the N−H bond, which continues until the transition state and reaches into the product region. The change in the nature of the reaction force near the minimum together with the increasing N−H distance indicate the onset of an electronic redistribution, which will be confirmed by the reaction electronic flux and the bond orders. The reaction force in the transition state region crosses zero and decreases linearly in the product region. The transition state region describes the travel of the hydrogen atom from the donor to acceptor atom keeping the distance between the nitrogen atom as donor and the oxygen atom as acceptor constant. This process is dominated by electronic changes. In the product region the reaction force adopts again a linear behavior with almost fixed O−H distance and the two monomers separate from each other. The much smaller structural rearrangements needed in the product region go inline with a product like transition state in accordance with the Hammond postulate.

The chemical potential (Supporting Information) and the reaction electronic flux allow a more detailed description where electronic reorganization takes place along the reaction coordinate. As shown in Figure 3d, the almost zero electronic flux in the reactant region confirms the structural rearrangements needed and the low electronic activity taking place in this part of the potential energy surface. The point on the reaction coordinate, where the chemical potential changes and the electronic flux deviates from zero, matches the pronounced decrease of the reaction force ($\xi = -1.0$). This point describes the beginning of the electronic reorganization, which reaches into the transition state region. The energy prior to this point amounts to approximately 7.7 kcal/mol and constitutes only 39% of the activation barrier (6.6 kcal/mol or 33% taking the energy of the more rigorous focal point method) and can be safely associated to

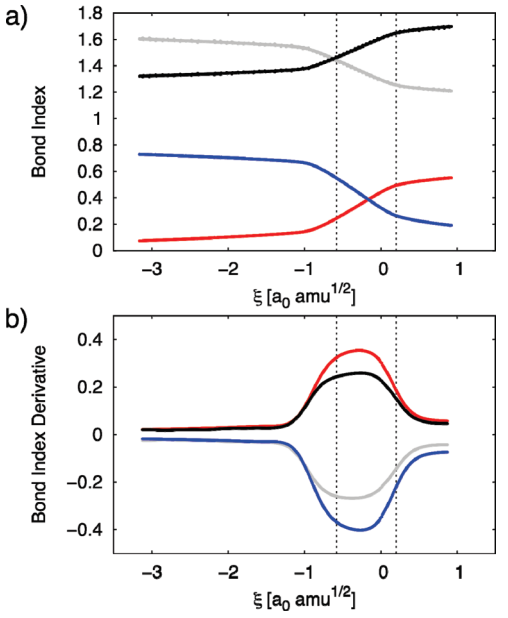

Figure 4. (a) Wiberg bond indices obtained from a NBO analysis: N−H bond (blue), O−H bond (red), C−N bond (black), and C−O bond (gray). (b) Derivative of the bond indices with respect to the reaction coordinate. Positive values represent bond formation, and negative values, bond rupture.

structural reordering that prepares the reaction. The chemical potential together with the reaction electronic flux shows that electronic reordering is necessary to reach the transition state region. This electronic activity is responsible for 67% of the activation barrier. The most substantial electronic reordering occurs in the transition state region. However, the conclusion of the electronic reordering extends to the product region. This assists in explaining the concerted nature of the reaction, showing

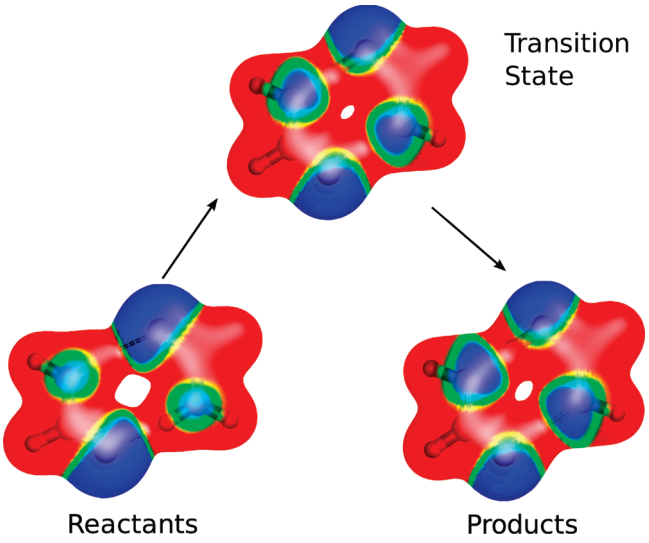

Figure 5. Electrostatic potential mapped on the electron density isosurface (isovalue = 0.01 e/a_0^3) for reactant, transition state, and product (red = +0.02 e and blue = −0.02 e).

that there is significant electronic redistribution along a considerable portion of the reaction coordinate.

The onset of the electronic reorganization characterized by the reaction electronic flux is also reflected in the bond indices and their derivatives (Figure 4a,b). Bond formation and rupture indicated by positive and negative derivative respectively, starts with the onset of the electronic reorganization reflected in the electronic flux and extends into the product region. Since the derivatives of the bonds between the carbon and nitrogen, or carbon and oxygen, atoms reach their maximum before the other two bonds, one may conclude that prior to the formation and rupture of the H-bonds between acceptor and donor a redistribution of the π-bond is required.

To visualize the electronic reorganization in the dimer, the electrostatic potential is mapped on the isosurface of the electron density for the reactant, the transition state, and the product in Figure 5 (at the B3LYP/6-311G(d,p) level). Positive regions are shown in red, and regions with a negative potential, in blue. The lone pairs of the electronegative oxygen in the reactant lead to a negative potential shown as a blue region, which is more negative than the nitrogen lone pair. The carbon atom lies in a positive region due to its cationic character in the carbonyl bond. When reaching the transition state and when in the product, the potential in the vicinity of the nitrogen atom gets more negative due to the transfer of the protons and is oriented in the direction of the oxygen and hydrogen atom of the other monomer.

This accumulation of electron density between the two monomers along the H-bonds is in accordance with smaller bond indices for the covalent donor hydrogen (O−H) and larger ones for the acceptor hydrogen (N−H) bonds in the product with respect to the reactant (Figure 4a). The bond index of the C−N bond with respect to the C═O bond in the reactant also increases. Additionally, the electron density between the two monomers in the imino ether product and the transition state is in agreement with the results of Grabowski et al.,[28] which reflect a larger delocalization energy term in the transition state and product than in the reactant. Hence, the treatment of nonbonded repulsion and electron delocalization are the key effects that govern this reaction. Further, the incorrect description of these leads directly to the discrepancies observed with DFT.

CONCLUSIONS

The combination of reaction force, reaction electronic flux, and NBO analysis with the focal point method provide a very accurate description of the energetic requirements for each part of the double proton transfer in the formamide dimer. The activation barrier consists of a smaller contribution characterized by pure structural rearrangements (33%) and a larger part that involves electronic reorganization (67%). The synchronous proton transfer is initiated through the approach of the two monomers, which is followed by electronic reorganization, activating the transfer of the two protons before reaching the transition state in accordance with the Hammond postulate. The delocalization of the electrons throughout the ring formed by the two monomers in the transition state is enhanced in the product due to the electronegativities of the involved oxygen and nitrogen atoms. This effect may be directly correlated to the error seen in the B3 exchange.

ASSOCIATED CONTENT

Supporting Information. Tables of focal points, energies, and atomic coordinates. Figure of chemical potentials along the reaction coordinate. This information is available free of charge via the Internet at http://pubs.acs.org.

ACKNOWLEDGMENT

E.V.M. thanks the Bundesministerium für Bildung und Forschung and the Alexander von Humboldt foundation for financial support. A.T.L. is thankful for support provided by Proyecto FONDECYT 1090460. J.C.H. and H.F.S. thank the U.S. National Science Foundation for funding. H.L.W. would like to thank NIH (1K22HL088341-01A1) and the University of South Florida (start-up) for funding.

REFERENCES

(1) Bell, R. P. *The Tunnel Effect in Chemistry*; Chapman and Hall: New York, 1980.
(2) Melander, L.; Saunders, W. H. J. *Reaction Rates of Isotopic Molecules*; John Wiley and Sons: New York, 1980.
(3) Bender, M. L. *Mechanisms of Homogeneous Catalysis from Protons to Proteins*; John Wiley and Sons: New York, 1971.
(4) Zielinski, T. J.; Poirier, R. A. *J. Comput. Chem.* **1984**, *5*, 466.
(5) Wang, X.-C.; Nichols, J.; Feyereisen, M.; Gutowski, M.; Boatz, J.; Haymet, A. D. J.; Simons, J. *J. Phys. Chem.* **1991**, *95*, 10419.
(6) Wójcik, M. J.; Hirakawa, A. Y.; Tsuboi, M.; Kato, S.; Morokuma, K. *J. Phys. Chem.* **1991**, *95*, 10419.
(7) Vargas, R.; Garza, J.; Friesner, R. A.; Stern, H.; Hay, B. P. *J. Phys. Chem. A* **2001**, *105*, 4963.
(8) Del Re, G.; Adamo, C. *J. Phys. Chem.* **1991**, *95*, 4231.
(9) Hrouda, V.; Florián, J.; Polášek, M.; Hobza, P. *J. Phys. Chem.* **1994**, *98*, 4742.
(10) Florián, J.; Leszczynski, J.; Johnson, B. G. *J. Mol. Struct.* **1995**, *349*, 421.
(11) Neuheuser, T.; Hess, B. A.; Reutel, C.; Weber, E. *J. Phys. Chem.* **1994**, *98*, 6459.
(12) Hobza, P.; Šponer, J. *J. Mol. Struct.* **1996**, *388*, 115.
(13) Cabaleiro-Lago, E. M.; Rios, M. A. *J. Chem. Phys.* **1999**, *110*, 6782.
(14) Hobza, P.; Havlas, Z. *Theor. Chem. Acc.* **1998**, *99*, 372.

(15) Colominas, C.; Luque, F. J.; Orozco, M. *J. Phys. Chem. A* **1999**, *103*, 6200.
(16) Gresh, N.; Guo, H.; Salahub, D. R.; Roques, B. P.; Kafafi, S. A. *J. Am. Chem. Soc.* **1999**, *121*, 7885.
(17) Brdarski, S.; Åstrand, P.-O.; Karlström, G. *Theor. Chem. Acc.* **2000**, *105*, 7.
(18) Podolyan, Y.; Gorb, L.; Leszczynski, J. *J. Phys. Chem. A* **2002**, *106*, 12103.
(19) Langley, C. H.; Allinger, N. L. *J. Phys. Chem. A* **2003**, *107*, 5208.
(20) Salvador, P.; Dannenberg, J. J. *J. Phys. Chem. B* **2004**, *108*, 15370.
(21) Bende, A.; Suhai, S. *Int. J. Quantum Chem.* **2005**, *103*, 841.
(22) Wu, Q.; Ayers, P. W.; Zhang, Y. *J. Chem. Phys.* **2009**, *131*, 164112.
(23) Florián, J.; Johnson, B. G. *J. Phys. Chem.* **1995**, *99*, 5899.
(24) Frey, J. A.; Leutwyler, S. *Chimia* **2005**, *59*, 511.
(25) Šponer, J.; Hobza, P. *J. Phys. Chem. A* **2000**, *104*, 4592.
(26) Kim, Y.; Lim, S.; Kim, J.-H.; Kim, Y. *J. Phys. Chem. A* **1999**, *103*, 617.
(27) Jurečka, P.; Hobza, P. *Chem. Phys. Lett.* **2002**, *265*, 89.
(28) Grabowski, S. J.; Sokalski, W. A.; Leszczynski, J. *J. Phys. Chem. A* **2006**, *110*, 4772.
(29) Tam, C. N.; Bour, P.; Eckert, J.; Trouw, F. R. *J. Phys. Chem. A* **1997**, *101*, 877.
(30) Ohtaki, H.; Funaki, A.; Rode, B. M.; Reibnegger, G. J. *J. Bull. Chem. Soc. Jpn.* **1983**, *56*, 2116.
(31) Lucas, B.; Grégoire, G.; Lecomte, F.; Reimann, B.; Schermann, J. P.; Desfrançois, C. *Mol. Phys.* **2005**, *103*, 1497.
(32) Cybulski, H.; Sadlej, J. *Phys. Chem. Chem. Phys.* **2009**, *11*, 11232.
(33) Herrera, B.; Toro-Labbé, A. *J. Phys. Chem. A* **2007**, *111*, 5921.
(34) Vöhringer-Martinez, E.; Toro-Labbé, A. *J. Comput. Chem.* **2010**, *31*, 2642.
(35) Lamsabhi, A. M.; Mó, O.; Gutiérrez-Oliva, S.; Pérez, P.; Toro-Labbé, A.; Yáñez, M. *J. Comput. Chem.* **2008**, *30*, 389.
(36) Fukui, K. *J. Mol. Struct.* **1981**, *14*, 363.
(37) Martinez, J.; Toro-Labbé, A. *J. Math. Chem.* **2009**, *45*, 911.
(38) Toro-Labbé, A. *J. Phys. Chem. A* **1999**, *103*, 4398.
(39) Jaque, P.; Toro-Labbé, A. *J. Phys. Chem. A* **2000**, *104*, 995.
(40) Toro-Labbé, A.; Gutiérrez-Oliva, S.; Murray, J. S.; Politzer, P. *Mol. Phys.* **2007**, *105*, 2619.
(41) Burda, J. V.; Toro-Labbé, A.; Gutiérrez-Oliva, S.; Murray, J. S.; Politzer, P. *J. Phys. Chem. A* **2007**, *111*, 2455.
(42) Jaque, P.; Toro-Labbé, A.; Politzer, P.; Geerlings, P. *Chem. Phys. Lett.* **2008**, *456*, 135.
(43) Vogt-Geisse, S.; Toro-Labbé, A. *J. Chem. Phys.* **2009**, *130*, 244308.
(44) Echegaray, E.; Toro-Labbé, A. *J. Phys. Chem. A* **2008**, *112*, 11801.
(45) Politzer, P.; Murray, J. S.; Lane, P.; Toro-Labbé, A. *Int. J. Quantum Chem.* **2007**, *107*, 2153.
(46) Politzer, P.; Toro-Labbé, A.; Gutiérrez-Oliva, S.; Herrera, B.; Jaque, P.; Concha, M. C.; Murray, J. *J. Chem. Sci.* **2005**, *117*, 467.
(47) Gutiérrez-Oliva, S.; Herrera, B.; Toro-Labbé, A.; Chermette, H. *J. Phys. Chem. A* **2005**, *109*, 1748.
(48) Sen, K. J.; Jorgensen, C. K. *Electronegativity: Structure and Bonding*; Springer-Verlag: Berlin, 1987; Vol. 66.
(49) Pearson, R. G. *Coord. Chem. Rev.* **1990**, *100*, 403.
(50) Pauling, L. *The Nature of the Chemical Bond*; Cornell University Press: New York, 1960.
(51) Pearson, R. G. *Hard and Soft Acids and Bases*; Dowden, Hutchinson, & Ross: Stroudsberg, PA, 1973.
(52) Pearson, R. G. *J. Am. Chem. Soc.* **1985**, *107*, 6801.
(53) Ayers, P. W.; Parr, R. *J. Am. Chem. Soc.* **2000**, *122*, 2010.
(54) Geerlings, P.; Proft, F. D.; Langenaeker, W. *Chem. Rev.* **2003**, *103*, 1793.
(55) East, A. L. L.; Allen, W. D. *J. Chem. Phys.* **1993**, *99*, 4638.
(56) Kenny, J. P.; Allen, W. D.; Schaefer, H. F. *J. Chem. Phys.* **2003**, *118*, 7353.
(57) Gonzales, J. M.; Pak, C.; Cox, R. S.; Allen, W. D.; Tarczay, G.; Császár, A. G. *Chem.—Eur. J.* **2003**, *9*, 2173.
(58) Császár, A. G.; Allen, W. D.; Schaefer, H. F. *J. Chem. Phys.* **1998**, *108*, 9751.
(59) Hargis, J. C. E., F. A.; Ingels, J. B.; Schaefer, H. F. *J. Am. Chem. Soc.* **2008**in press.
(60) Becke, A. D. *J. Chem. Phys.* **1993**, *98*, 5648.
(61) Lee, C. T.; Yang, W. T.; Parr, R. G. *Phys. Rev. B* **1988**, *37*, 785.
(62) Foster, J. P.; Weinhold, F. *J. Am. Chem. Soc.* **1980**, *102*, 7211.
(63) Reed, A. E.; Curtiss, L. A.; Weinhold, F. *Chem. Rev.* **1988**, *88*, 899.
(64) Glendening, E. D.; Reed, A. E.; Carpenter, J. E.; Weinhold, F. *NBO*, 3.1 ed.; Theoretical Chemistry Institute, University of Wisconsin: Madison, WI, 1994.
(65) Frisch, M. J.; Trucks, G. W.; Schlegel, H. B.; Scuseria, G. E.; Robb, M. A.; Cheeseman, J. R.; Montgomery, J. A., Jr.; Vreven, T.; Kudin, K. N.; Burant, J. C.; Millam, J. M.; Iyengar, S. S.; Tomasi, J.; Barone, V.; Mennucci, B.; Cossi, M.; Scalmani, G.; Rega, N.; Petersson, G. A.; Nakatsuji, H.; Hada, M.; Ehara, M.; Toyota, K.; Fukuda, R.; Hasegawa, J.; Ishida, M.; Nakajima, T.; Honda, Y.; Kitao, O.; Nakai, H.; Klene, M.; Li, X.; Knox, J. E.; Hratchian, H. P.; Cross, J. B.; Bakken, V.; Adamo, C.; Jaramillo, J.; Gomperts, R.; Stratmann, R. E.; Yazyev, O.; Austin, A. J.; Cammi, R.; Pomelli, C.; Ochterski, J. W.; Ayala, P. Y.; Morokuma, K.; Voth, G. A.; Salvador, P.; Dannenberg, J. J.; Zakrzewski, V. G.; Dapprich, S.; Daniels, A. D.; Strain, M. C.; Farkas, O.; Malick, D. K.; Rabuck, A. D.; Raghavachari, K.; Foresman, J. B.; Ortiz, J. V.; Cui, Q.; Baboul, A. G.; Clifford, S.; Cioslowski, J.; Stefanov, B. B.; Liu, G.; Liashenko, A.; Piskorz, P.; Komaromi, I.; Martin, R. L.; Fox, D. J.; Keith, T.; Al-Laham, M. A.; Peng, C. Y.; Nanayakkara, A.; Challacombe, M.; Gill, P. M. W.; Johnson, B.; Chen, W.; Wong, M. W.; Gonzalez, C.; Pople, J. A. *Gaussian 03*, 02 ed.; Gaussian Inc.: Wallingford, CT, 2004.
(66) Dunning, T. H. *J. Chem. Phys.* **1970**, *53*, 2823.
(67) Feller, D. *J. Chem. Phys.* **1993**, *98*, 7059.
(68) Helgaker, T.; Klopper, W.; Koch, H.; Noga, J. *J. Chem. Phys.* **1997**, *106*, 9639.
(69) Werner, H.-J.; Knowles, P. J.; Lindh, R.; Manby, F. R.; Schütz, M.; Clelani, P.; Korona, T.; Rauhut, G.; Amos, R. D.; Bernhardsson, A.; Berning, A.; Cooper, D. L.; Deegan, M. J. O.; Dobbyn, A. J.; Eckert, F.; Hampel, C.; Hetzer, G.; Lloyd, A. W.; McNicholas, S. J.; Meyer, W.; Mura, M. E.; Nicklass, A.; Palmieri, P.; Pitzer, R.; Schumann, U.; Stoll, H.; Stone, A. J.; Tarroni, R.; Thorsteinsson, T. *Molpro*, 2006.1 ed.; Universität Stuttgart and Cardiff University, 2006.
(70) Lindh, R.; Ryu, U.; Liu, B. *J. Chem. Phys.* **1991**, *95*, 5889.
(71) Hampel, C.; Peterson, K. A.; Werner, H. J. *Chem. Phys. Lett.* **1992**, *190*, 1.
(72) Shao, Y.; Molnar, L. F.; Jung, Y.; Kussmann, J.; Ochsenfeld, C.; Brown, S. T.; Gilbert, A. T. B.; Slipchenko, L. V.; Levchenko, S. V.; O'Neill, D. P.; DiStasio, R. A.; Lochan, R. C.; Wang, T.; Beran, G. J. O.; Besley, N. A.; Herbert, J. M.; Lin, C. Y.; Van Voorhis, T.; Chien, S. H.; Sodt, A.; Steele, R. P.; Rassolov, V. A.; Maslen, P. E.; Korambath, P. P.; Adamson, R. D.; Austin, B.; Baker, J.; Byrd, E. F. C.; Dachsel, H.; Doerksen, R. J.; Dreuw, A.; Dunietz, B. D.; Dutoi, A. D.; Furlani, T. R.; Gwaltney, S. R.; Heyden, A.; Hirata, S.; Hsu, C. P.; Kedziora, G.; Khalliulin, R. Z.; Klunzinger, P.; Lee, A. M.; Lee, M. S.; Liang, W.; Lotan, I.; Nair, N.; Peters, B.; Proynov, E. I.; Pieniazek, P. A.; Rhee, Y. M.; Ritchie, J.; Rosta, E.; Sherrill, C. D.; Simmonett, A. C.; Subotnik, J. E.; Woodcock, H. L.; Zhang, W.; Bell, A. T.; Chakraborty, A. K.; Chipman, D. M.; Keil, F. J.; Warshel, A.; Hehre, W. J.; Schaefer, H. F.; Kong, J.; Krylov, A. I.; Gill, P. M. W.; Head-Gordon, M. *Phys. Chem. Chem. Phys.* **2006**, *8*, 3172.
(73) Kobayashi, Y.; Kamiya, M.; Hirao, K. *Chem. Phys. Lett.* **2000**, *319*, 695.
(74) Gritsenko, O. V.; Ensing, B.; Schipper, P. R. T.; Baerends, E. J. *J. Phys. Chem. A* **2000**, *104*, 8558.
(75) Larkin, J. D.; Bhat, K. L.; Markham, G. D.; Brooks, B. R.; Schaefer, H. F.; Bock, C. W. *J. Phys. Chem. A* **2006**, *110*, 10633.

(76) Moran, D.; Simmonett, A. C.; Leach, F. E.; Allen, W. D.; Schleyer, P. v. R.; Schaefer, H. F. *J. Am. Chem. Soc.* **2006**, *128*, 9342.
(77) Johnson, E. R.; Mori-Sánchez, P.; Cohen, A. J.; Yang, W. *J. Chem. Phys.* **2008**, *129*, 204112.
(78) Woodcock, H. L.; Schaefer, H. F.; Schreiner, P. R. *J. Phys. Chem. A* **2002**, *106*, 11923.
(79) B3-noLYP is B3LYP without LYP correlation. It is the B3 exchange term.